Intermetallics 84 (2017) 74–81

Contents lists available at ScienceDirect

Intermetallics

journal homepage: www.elsevier.com/locate/intermet

Saturated magnetization and glass forming ability of soft magnetic Fe-based metallic glasses

B. Huang [a], Y. Yang [a, *], A.D. Wang [b], Q. Wang [c], C.T. Liu [a, **]

[a] Centre for Advanced Structural Materials, Department of Mechanical and Biomedical Engineering, City University of Hong Kong, Tat Chee Avenue, Kowloon Tong, Kowloon, Hong Kong Special Administrative Region
[b] Key Laboratory of Magnetic Materials and Devices, Ningbo Institute of Materials Technology and Engineering, Chinese Academy of Sciences, Ningbo, Zhejiang, 315201, China
[c] Laboratory for Microstructures, Institute of Materials Science, Shanghai University, Shanghai, 200072, China

ARTICLE INFO

Article history:
Received 3 April 2016
Received in revised form
21 August 2016
Accepted 3 January 2017
Available online 10 January 2017

Keywords:
Metallic glasses
Magnetic properties
Glass forming ability
Microstructure

ABSTRACT

Saturated magnetization (B_s) and glass forming ability (GFA) are two important attributes of soft magnetic metallic glasses (MGs), both of which are affected by the local short-range order in amorphous structures. Based on the notion of free electron transfer, we propose a set of simple rules for the calculation of B_s from the chemical composition of soft magnetic Fe-based alloys. Through the comparison of the experimentally measured B_s and theoretically calculated B_s, we show that the soft magnetic Fe-based MGs can be generally categorized into two types: one has its GFA correlated positively with the ferromagnetic weakness and the other has its GFA correlated negatively with the ferromagnetic weakness. Finally, the structural mechanisms behind these correlations are discussed.

© 2017 Elsevier Ltd. All rights reserved.

1. Introduction

Owing to their low energy waste, soft magnetic metallic glasses (MGs) with excellent properties, such as high saturated magnetic flux density (B_s), low coercivity (H_c) and high permeability (μ), are of great potential to be used in various electric devices, such as transformers, reactors, motors, and mutual inductors, as a replacement of traditional crystalline materials, like silicon steel [1–3]. Further improvement of their magnetic properties has been attracting tremendous research interest, motivating the continuing search of MGs with larger B_s lower H_c and μ. Since 1980s, soft magnetic amorphous and nanocrystalline alloys with hundreds of compositions have been explored [2,4–6], which usually contain various nonmagnetic metallic elements, such as Nb, Zr and Mo, and even non-metallic elements, such as P and C. However, compared to silicon steels (containing 6.5 mass% Si) with B_s~1.85 T, the B_s of most of these alloys is low, which is generally lower than 1.7 T [7–9]. For instance, the $Fe_{73.5}Si_{13.5}B_9Nb_3Cu_1$ alloy has a rather low B_s (~1.24 T). Recently, FeCuSiB [10] and FeSiBPCu [11] soft magnetic alloys with nanocrystal precipitations were developed, exhibiting a high B_s (>1.8 T) close to that of silicon steels.

In principle, B_s of an alloy arises from the magnetic moments of its composing atoms. According to the well-known Slater-Pauling curves [12], the compositionally dependent average magnetic moment $\bar{\mu}$ of 3*d*-transitional-metal-based alloys can be attributed to the unpaired electron spins. From the picture of the rigid-band model [12], $\bar{\mu}$ may be simply written as $(N_\uparrow - N_\downarrow)\ \mu_B$ with $N_\uparrow$ the up-spin valence electron number, $N_\downarrow$ the down-spin valence electron number and μ_B the Bohr magnetron. Suppose that the total valence electron number $Z = N_\uparrow + N_\downarrow$, one can thus obtain $\bar{\mu} = (2N_\uparrow - Z)\cdot\mu_B$ for strongly magnetic alloys with the up-spin band filled and the $N_\uparrow$ constant, which explains the downward 45° trend-line with in plot of the Slater–Pauling curves [12]. However, for weakly magnetic alloys with the up-spin band unfilled, $N_\downarrow$ remains constant with alloying because the Fermi level was considered to be pinned at the band gap of the spin-down electrons. In this case, one obtains $\bar{\mu} = (Z - 2N_\downarrow)g\mu_B$ and this equation simply explains the upward 45° trend line in the plot of the Slater–Pauling curves [12]. Nevertheless, the later sophisticated calculations and experiments suggested that the electron bands are not really 'rigid' even for the simplest case [13]. The first

* Corresponding author.
** Corresponding author.
E-mail addresses: yonyang@cityu.edu.hk (Y. Yang), chainliu@cityu.edu.hk (C.T. Liu).

http://dx.doi.org/10.1016/j.intermet.2017.01.003
0966-9795/© 2017 Elsevier Ltd. All rights reserved.

major modification of the rigid-band picture came from the work of Friedel [14], who recognized that, in mixtures of early and late transition metals, the relatively repulsive *d* potential in the early transition-metal solute creates a separate high-energy *d* band containing precisely five virtual bound states above the Fermi level per solute. This theory accounts for the non-45°-slope subbranches in the plot of the Slater-Pauling curves, mainly for the Ni- and Co-based alloys. As for the alloys containing metalloid, the constancy of $N_{sp,\uparrow}$, i. e., the number of spin-up *sp* electrons, and also $N_{\uparrow}$ are also debated. For the possible variation of $N_{sp,\uparrow}$ and $N_{\uparrow}$, different theories and models, such as the band-gap theory [15], the charge transfer theory [16] and the generalized Slater-Pauling plot [17], were proposed for crystalline and amorphous metallic alloys. Parameter-free and self-consistent band calculations also indicated the magnetic weakness of Fe- and Co-based amorphous alloys mixed with early transitional metals, in which the up-spin *d* bands are not always fully filled [18]. Single site theory, the theory of local environment effects and the finite-temperature theory were proposed to calculate the magnetization of amorphous alloys in a more accurate manner [12,19]. Today, it is recognized that the deviation from the Slater-Pauling curves originates from the variation of local short-range structures; however, it is still far from being clear how the local short-range structures could possibly influence the B_s across various MGs [2,8].

On the other hand, glass forming ability (GFA) is an important property of MGs describing their ability of restraining from crystal nucleation for the corresponding undercooled liquids upon quenching. Experiments and simulations revealed that GFA of MGs is closely correlated with the local symmetry of atomic clusters [20,21], the atomic- and cluster-level packing efficiency [22], the density change upon crystallization [23] and even the density of electronic energy states at the Fermi level [24]. Since both GFA and B_s of MGs are related to the local atomic packing, it is intriguing to examine whether and/or how GFA and B_s are connected with each other. In this letter, we would first propose a simple model to calculate the $\overline{\mu}$ of soft-magnetic MGs, in a similar spirit of the rigid-band model [12], based on the transfer of free electrons from the element with a high chemical potential or Fermi level (E_F) to that with a lower chemical potential. This would serve as a reference case, without considering the influence of the local short-range structures, to be compared to the real experimental measurements. Subsequently, we will show that the deviation of the experimental B_s from the calculated results is indeed, either positively or negatively, correlated with the GFA as quantified by the thermodynamic parameter T_{rg} ($T_{rg} = T_g/T_l$, where T_g and T_l are the glass transition temperature and the liquidus temperature respectively). Our findings shed quantitative insight into the effect of local atomic packing variation on the saturated magnetization in MGs across different compositions, which could guide the design of soft-magnetic MGs with controlled B_s and GFA.

2. Results and discussions

2.1. Simple rules of free electron transfer

From the perspective of valence electrons, at the contact of two metals with different E_F, electrons are transferred from the high-E_F metal to the low-E_F one till the E_F's of the two are equal. If we assume that such a picture of valence electron transfer is valid for Fe-based alloys, we may calculate the magnetization of the alloys based on the E_F of the constituent elements. The difference of the number of the up-spin electrons $N_{\uparrow}$ ($N_{\uparrow} = 5$) and the down-spin electrons $N_{\downarrow}$ ($N_{\downarrow} = 2.78$) in the *d* band is known to be 2.22 for ferromagnetic bcc iron, and we simply regard that the average magnetic moment of Fe atoms $\overline{\mu}_{Fe}$ in a ferromagnetic Fe-based MG is also 2.22 μ_B according to the reported experimental data as shown in Fig. 1(a) [5,16]. If the element M with a higher E_F is alloyed into the alloy, part of its electrons will transfer into Fe till the E_F's of Fe and the alloyed element are equal. As a result, $N_{\downarrow}$ increases and $\overline{\mu}_{Fe}$ decreases and *vice versa*, as shown in Fig. 1(b). Meanwhile, the filling of the energy band of M will also be changed due to the transfer of electrons. Based on the above general consideration, the

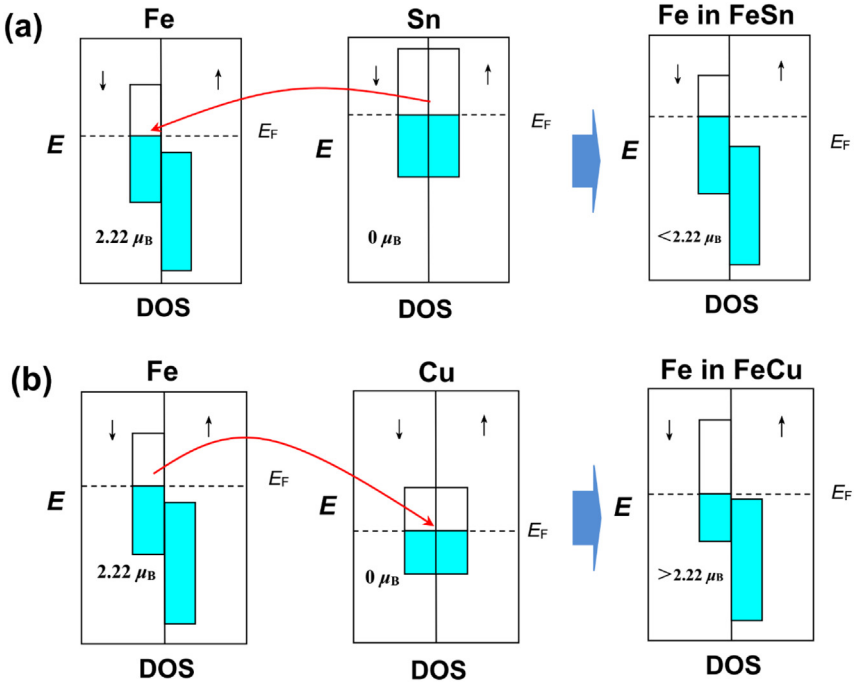

Fig. 1. (a) The change of the *d* band of Fe in the Fe-based alloy with the addition of Sn. (b) The change of the *d* band of Fe in the Fe-based alloy with the addition of Cu. (A two-column fitting image.)

following scenarios are examined for the alloying of different types of elements with the atomic concentration x.

(1) M is a non-ferromagnetic metal at room temperature (RT). If the E_F of M is larger than Fe, free electrons of M will be transferred into Fe causing the reduction of $\overline{\mu}_{Fe}$. Since usually only a small amount of M is alloyed, we can reasonably suppose all the valence electrons of M are transferred into Fe. In addition, the alloying of M also dilutes the magnetic moments of iron in the alloy. As a result, the average magnetic moment $\overline{\mu}$ of the alloy $Fe_{1-x}M_x$ can be approximately calculated as $\overline{\mu} = (1-x)\overline{\mu}_{Fe} + nx\cdot\mu_B$, where n is negative and $-n$ is the number of valance electrons per M atom. Elements of this type include Al, Sc, Ti, V, Cr, Mn, Zn, Zr, Nb, Mo, Ta, Sn, Bi and rare earth (RE) elements. Fig. 1(a) shows the d band change of Fe with the alloying of Sn with a zero magnetic moment. Similarly, if E_F of M is smaller than bcc Fe, free electrons transfer from Fe to M with alloying. We suppose all the holes of M in d band will be filled considering the small concentration of M. In this case, we also obtain $\overline{\mu} = (1-x)\overline{\mu}_{Fe} + nx\cdot\mu_B$ for a $Fe_{1-x}M_x$ alloy, where n is positive and equals to the average number of holes in d band per M atom. Cu, Pd, Au and other noble elements belong to this type. Fig. 1(b) shows the d band change of Fe with the alloying of Cu ($\overline{\mu}_{Cu}$=0). (2) M is ferromagnetic at RT with a non-zero $\overline{\mu}_M$ in the alloy. If M possesses a smaller E_F than Fe, we obtain $\overline{\mu}$= (1-x)$\overline{\mu}_{Fe}$+ $nx\mu_B$ + $x\overline{\mu}_M$-$nx\mu_B$= (1-x)$\overline{\mu}_{Fe}$+ $x\overline{\mu}_M$ for a $Fe_{1-x}M_x$ alloy, where n is positive and equals to the average number of holes in d band per M atom. Elements like Co and Ni belong to this type. Evidently, the result is the same for the alloying of a ferromagnetic metallic element with E_F larger than Fe. (3) M is a metalloid element with E_F different from that of Fe. For this case, we do not consider any electron transfer between M and Fe because of the lack of a fully established metallic bond. Note that this treatment is different from the charge transfer theory for metal-metalloid alloys, in which $\overline{\mu}$ of the alloy decreases by mx μ_B with m being the average number of free electrons transferred from every M to iron [16]. The commonly used B, C, Si and P are considered to be this kind of elements. Furthermore, it can be demonstrated that the above rules set for our calculation of $\overline{\mu}$ of the alloys without metalloids are equivalent to those of the rigid-band model and the virtual-bound-state theory of Friedel [12]. Now, we are at the position to analyze the saturated magnetization of multicomponent Fe-based soft magnetic alloys without considering the local structure effect.

Fig. 2(a) and (b) show respectively the E_F [25] and n of the typical elements composing the soft-magnetic alloys. In the figures, the elements transferring electrons to the matrix Fe element are marked as “Donor”, and those accepting electrons from the matrix are marked as “Acceptor”. With the data and the aforementioned rules, we can calculate $\overline{\mu}$ for a variety of soft-magnetic alloys, which are listed in Table 1 together with the experimentally measured B_s. Here, B_s represents the density of magnetic dipoles in an alloy, which can be expressed as $B_s = N_A\overline{\mu}\mu_B/V_m$, where N_A and V_m denote the Avogadro number and the molar volume of the alloy, respectively. In theory, we can write $\overline{\mu}$= $(V_m/N_A\mu_B)B_s$=$(V_m/V_{m,Fe})(V_{m,Fe}/N_A\mu_B)B_s$, where $V_{m,Fe}$ (=7.092×10^{-6} m^3) is the molar volume of bcc iron. For the studied Fe-based soft magnetic alloys, the concentration of Fe varies from ~50% to 100% with a low concentration of nonmagnetic elements and thus, we may take $V_m/V_{m,Fe} \approx 1$ as an approximation, which then leads to a simple correlation between $\overline{\mu}$ and B_s:

$$\overline{\mu} = \left(\frac{V_{m,Fe}}{N_A\mu_B}\right)B_s \quad (1)$$

If the electron transfer model is suitable for Fe-based alloys, the calculated $\overline{\mu}$ and experimental B_s should lie on the grey dashed line described by Eq. (1). Fig. 3 shows the plot of the calculated $\overline{\mu}$ versus

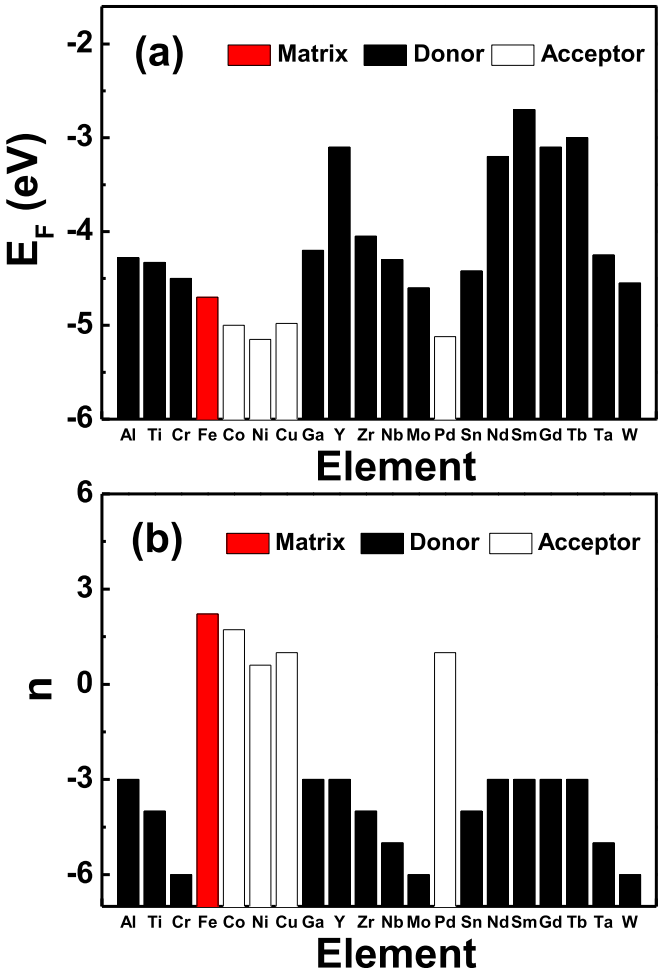

Fig. 2. (a) The Fermi energy E_F of different elements. (b) The n of typical elements used for the calculations. (A single column fitting image.)

experimental B_s, from which one can clearly see a strong correlation between $\overline{\mu}$ and B_s (see the red dashed line). This behavior suggests that electron transfer does play a role in the saturated magnetization of various Fe-based alloys and our theoretical model, albeit its simplicity, captures the major trend exhibited by the experimental data. However, a departure from Eq. (1) (depicted as the grey dashed line) is also noted in Fig. 3, especially for the Fe-based MGs, which suggests the calculated $\overline{\mu}$ and the corresponding calculated saturated magnetization are larger that the experimental values. Eq. (1) is suitable for the Fe-based nanocrystalline and crystalline alloys with a high concentration of Fe (For the convenience of discussions, the studied Fe-based alloys are divided into ordinary Fe-, FeCo-, FeCoRE-, FeNi-, FeCoNi-based MGs, Fe-based nanocrystalline and crystalline alloys according to the type of the alloyed element and the structure of the alloy as listed in Table 1). This phenomenon signals a plausible effect of local structures for MGs which is not considered in our simple model.

2.2. Departure from the electron-transfer model and local structure effect

Now, let us discuss the possible structural mechanisms for the departure of the experimental data from the free electron rule, as seen in Fig. 3. Based on the literature results [18], it is known that, unlike ferromagnetic bcc Fe with $\overline{\mu}$ = 2.22 μ_B, Fe atoms are antiferromagnetic if arranged in a closely packed configuration, such as

Table 1
The experimental saturated magnetization B_s and calculated average magnetic moment $\overline{\mu}$ for Fe-based MGs, nanocrystalline and crystalline alloys.

Composition	B_s (T)	$\overline{\mu}$ (A m^2)
Ordinary Fe-		
$Fe_{79}P_{10}C_4B_4Si_3$ [34]	1.53	1.75
$Fe_{78}Mo_1P_{10}C_4B_4Si_3$ [34]	1.44	1.67
$Fe_{77}Mo_2P_{10}C_4B_4Si_3$ [34]	1.39	1.59
$Fe_{76}Mo_3P_{10}C_4B_4Si_3$ [34]	1.32	1.50
$Fe_{75}Mo_4P_{10}C_4B_4Si_3$ [34]	1.27	1.42
$Fe_{74}Mo_5P_{10}C_4B_4Si_3$ [34]	1.14	1.34
$Fe_{75}Mo_5P_{10}C_{7.5}B_{2.5}$ [34]	1.10	1.36
$Fe_{76}C_{7.0}Si_{3.3}B_5P_{8.7}Mo_0$ [35]	1.52	1.68
$Fe_{75}C_{7.0}Si_{3.3}B_5P_{8.7}Mo_1$ [35]	1.41	1.60
$Fe_{73}C_{7.0}Si_{3.3}B_5P_{8.7}Mo_3$ [35]	1.30	1.44
$Fe_{71}C_{7.0}Si_{3.3}B_5P_{8.7}Mo_5$ [35]	1.10	1.27
$(Fe_{0.76}Si_{0.096}B_{0.084}P_{0.06})_{100}Mo_0$ [26]	1.51	1.68
$(Fe_{0.76}Si_{0.096}B_{0.084}P_{0.06})_{98}Mo_2$ [26]	1.35	1.53
$(Fe_{0.76}Si_{0.096}B_{0.084}P_{0.06})_{96}Mo_4$ [26]	1.10	1.50
$(Fe_{0.76}Si_{0.096}B_{0.084}P_{0.06})_{94}Mo_6$ [26]	0.98	1.46
$Fe_{76}Mo_2Ga_2P_{10}C_4B_4Si_2$ [40]	1.32	1.50
$Fe_{74}Mo_4Ga_2P_{10}C_4B_4Si_2$ [40]	1.16	1.34
$Fe_{75}Mo_2Ga_3P_{10}C_4B_4Si_2$ [40]	1.27	1.45
$Fe_{73}Mo_4Ga_3P_{10}C_4B_4Si_2$ [40]	1.11	1.29
$(Fe_{75}B_{15}Si_{10})_{99}Nb_1$ [41]	1.50	1.60
$(Fe_{0.75}B_{0.15}Si_{0.10})_{98}Nb_2$ [41]	1.47	1.53
$(Fe_{0.75}B_{0.15}Si_{0.10})_{96}Nb_4$ [41]	1.40	1.40
$(Fe_{0.39}Ni_{0.39}B_{0.16}P_{0.06})_{99}Nb_1$ [36]	0.80	1.04
$(Fe_{0.39}Ni_{0.39}B_{0.16}P_{0.06})_{98.5}Nb_{1.5}$ [36]	0.77	1.01
$(Fe_{0.39}Ni_{0.39}B_{0.16}P_{0.06})_{98}Nb_2$ [36]	0.75	0.98
$(Fe_{0.39}Ni_{0.39}B_{0.16}P_{0.06})_{97.5}Nb_{2.5}$ [36]	0.73	0.95
$(Fe_{0.39}Ni_{0.39}B_{0.16}P_{0.06})_{97}Nb_3$ [36]	0.71	0.92
$(Fe_{0.39}Ni_{0.39}B_{0.16}P_{0.06})_{96}Nb_4$ [36]	0.66	0.86
$Fe_{73}Al_5Ga_2P_{11}C_5B_4$ [42]	1.14	1.41
$Fe_{72}Al_5Ga_2P_{10}C_6B_4Si_1$ [40]	1.07	1.39
$Fe_{74}Al_4Sn_2P_{10}Si_4B_4C_2$ [43]	1.31	1.44
$Fe_{74}Al_4Sn_2P_6Si_4B_4C_6$ [43]	1.37	1.44
$Fe_{75}Ga_5P_{12}C_4B_4$ [44]	1.27	1.51
$Fe_{77}Ga_3P_{9.5}C_4B_4Si_{2.5}$ [45]	1.36	1.62
$Fe_{78}Ga_2P_{9.5}C_4B_4Si_{2.5}$ [45]	1.40	1.67
$Fe_{80}P_9C_8B_2Si_1$ [46]	1.55	1.77
$Fe_{79}Sn_1P_9C_8B_2Si_1$ [46]	1.51	1.71
$Fe_{78}Sn_2P_9C_8B_2Si_1$ [46]	1.46	1.65
$Fe_{77}Sn_3P_9C_8B_2Si_1$ [46]	1.42	1.59
$Fe_{76}Si_{10}B_{10}Cr_2Y_2$ [33]	1.37	1.50
$Fe_{74}Y_3Nb_6B_{17}$ [47]	0.81	1.25
$(Fe_{0.74}Tb_{0.01}B_{0.2}Si_{0.05})_{96}Nb_4$ [38]	1.14	1.35
$(Fe_{0.73}Tb_{0.02}B_{0.2}Si_{0.05})_{96}Nb_4$ [38]	1.01	1.30
$(Fe_{0.72}Tb_{0.03}B_{0.2}Si_{0.05})_{96}Nb_4$ [38]	0.92	1.25
$(Fe_{0.71}Tb_{0.04}B_{0.2}Si_{0.05})_{96}Nb_4$ [38]	0.76	1.20
$(Fe_{0.70}Tb_{0.05}B_{0.2}Si_{0.05})_{96}Nb_4$ [38]	0.69	1.15
$(Fe_{0.69}Tb_{0.06}B_{0.2}Si_{0.05})_{96}Nb_4$ [38]	0.61	1.10
$(Fe_{0.68}Tb_{0.07}B_{0.2}Si_{0.05})_{96}Nb_4$ [38]	0.52	1.05
FeCo-		
$Fe_{67.7}C_{7.0}Si_{3.3}B_{5.5}P_{8.7}Cr_{2.3}Mo_{2.5}Al_{2.0}Co_1$ [48]	0.80	1.17
$Fe_{63.7}C_{7.0}Si_{3.3}B_{5.5}P_{8.7}Cr_{2.3}Mo_{2.5}Al_{2.0}Co_5$ [48]	0.85	1.15
$[(Fe_{0.9}Co_{0.1})_{0.75}B_{0.2}Si_{0.05}]_{96}Nb_4$ [49]	1.13	1.36
$[(Fe_{0.8}Co_{0.2})_{0.75}B_{0.2}Si_{0.05}]_{96}Nb_4$ [49]	1.05	1.32
$[(Fe_{0.7}Co_{0.3})_{0.75}B_{0.2}Si_{0.05}]_{96}Nb_4$ [49]	0.98	1.29
$[(Fe_{0.6}Co_{0.4})_{0.75}B_{0.2}Si_{0.05}]_{96}Nb_4$ [49]	0.93	1.25
$[(Fe_{0.5}Co_{0.5})_{0.75}B_{0.2}Si_{0.05}]_{96}Nb_4$ [49]	0.84	1.22
$[(Co_{0.6}Fe_{0.4})_{0.75}B_{0.2}Si_{0.05}]_{96}Nb_4$ [50]	0.97	1.18
$[(Co_{0.7}Fe_{0.3})_{0.75}B_{0.2}Si_{0.05}]_{96}Nb_4$ [50]	0.91	1.14
$[(Co_{0.8}Fe_{0.2})_{0.75}B_{0.2}Si_{0.05}]_{96}Nb_4$ [50]	0.78	1.11
$[(Co_{0.9}Fe_{0.1})_{0.75}B_{0.2}Si_{0.05}]_{96}Nb_4$ [50]	0.71	1.07
FeCoRE-		
$Fe_{62}Co_{9.5}Nd_3Dy_{0.5}B_{25}$ [51]	1.41	1.43
$Fe_{60.3}Co_{9.2}Nd_3Dy_{0.5}B_{25}Nb_2$ [52]	1.15	1.29
$Fe_{62}Co_{9.5}Pr_{3.5}B_{25}$ [51]	1.36	1.43
$Fe_{62}Co_{9.5}Sm_{3.5}B_{25}$ [51]	1.35	1.43
$Fe_{62}Co_{9.5}Gd_{3.5}B_{25}$ [51]	1.41	1.43
$Fe_{62}Co_{9.5}Dy_{3.5}B_{25}$ [51]	1.43	1.43
$Fe_{62}Co_{9.5}Tb_{3.5}B_{25}$ [51]	1.36	1.43
$Fe_{62}Co_{9.5}Er_{3.5}B_{25}$ [51]	1.38	1.43
FeNi-		
$Fe_{40}Ni_{40}P_{14}B_6$ [53]	0.86	1.13
$(Fe_{40}Ni_{40}P_{14}B_6)_{96}Ga_4$ [54]	0.75	0.97

Table 1 (*continued*)

Composition	B_s (T)	$\overline{\mu}$ (A m^2)
$Fe_{76}Mo_{3.5}P_{10}C_4B_4Si_{2.5}$ [39]	1.21	1.47
$Fe_{71}Ni_5Mo_{3.5}P_{10}C_4B_4Si_{2.5}$ [39]	1.17	1.39
$Fe_{66}Ni_{10}Mo_{3.5}P_{10}C_4B_4Si_{2.5}$ [39]	1.12	1.31
$Fe_{61}Ni_{15}Mo_{3.5}P_{10}C_4B_4Si_{2.5}$ [39]	1.03	1.23
$Fe_{56}Ni_{20}Mo_{3.5}P_{10}C_4B_4Si_{2.5}$ [39]	0.93	1.15
FeCoNi-		
$Fe_{56}Co_7Ni_7Zr_{10}B_{20}$ [55]	0.96	1.00
$Fe_{56}Co_7Ni_7Zr_8Nb_2B_{20}$ [55]	0.75	0.98
$Fe_{61}Co_7Ni_7Zr_8Nb_2B_{15}$ [55]	0.85	1.10
$[(Fe_{0.6}Co_{0.3}Ni_{0.1})_{0.75}B_{0.2}Si_{0.05}]_{95}Nb_4Zr_1$ [56]	0.60	1.12
$[(Fe_{0.8}Co_{0.1}Ni_{0.1})_{0.75}B_{0.2}Si_{0.05}]_{96}Nb_4$ [57]	1.10	1.24
$[(Fe_{0.6}Co_{0.1}Ni_{0.3})_{0.75}B_{0.2}Si_{0.05}]_{96}Nb_4$ [57]	0.80	1.01
$[(Fe_{0.6}Co_{0.2}Ni_{0.2})_{0.75}B_{0.2}Si_{0.05}]_{96}Nb_4$ [57]	0.86	1.09
$[(Fe_{0.6}\ Co_{0.3}\ Ni_{0.1})_{0.75}B_{0.2}Si_{0.05}]_{96}Nb_4$ [57]	0.90	1.17
Nanocrystalline		
$Fe_{83.5}B_{10}C_6Cu_{0.5}$ [58]	1.74	1.86
$Fe_{83}B_{10}C_6Cu_1$ [58]	1.78	1.85
$Fe_{82.7}B_{10}C_6Cu_{1.3}$ [58]	1.83	1.85
$Fe_{83.7}Cu_{1.5}B_{14.8}$ [58]	1.82	1.87
$Fe_{83.3}Si_4B_8P_4Cu_{0.7}$ [58]	1.88	1.85
$Fe_{82.75}Si_4B_8P_4Cu_{1.25}$ [59]	1.83	1.85
$Fe_{83}Si_4B_8P_4Cu_1$ [59]	1.82	1.85
$Fe_{82.65}Si_2B_9P_5Cu_{1.35}$ [60]	1.80	1.85
$Fe_{73.5}Si_{13.5}B_9Nb_3Cu_1$ [60]	1.24	1.49
$Fe_{90}Zr_7B_3$ [60]	1.70	1.75
Crystalline		
Fe (bcc) [32]	2.20	2.22
Fe-3 mass% Si [59]	2.03	2.15
Fe-6.5 mass% Si [59]	1.85	2.07

face-centered-cubic (fcc) lattice, or magnetically weak with $\overline{\mu}< 0.5$ μ_B in an amorphous structure. According to the band gap theory of strong ferromagnetism [15,18], the ferromagnetism of amorphous Fe-based alloys is related to structural "impurities", which strongly suppress the state density peak at the top of the *d* band of neighboring Fe atoms and thus results in a band gap above the Fermi level. The states at the Fermi level accumulate, which induces ferromagnetism when the state density at the Fermi level is raised above the critical Stoner value [12]. As the band gap pins the Fermi level of the up-spin *d* band and keeps $N_\uparrow$ as a constant, the number of down-spin electrons $N_\downarrow$ determines the ferromagnetism and the alloy is strongly magnetic. It is obvious that our simple free electron transfer model of magnetic MGs rests on the assumption of the band gap theory and strong ferromagnetism of the alloys. Based on Friedel's picture [14], the ferromagnetism strength is influenced by two factors. One is the impurity concentration, the increase of which leads to the smearing of the state density gap and thus affects the pinning of the Fermi level of the up-spin *d* band electrons [15]. The other is the distance of neighboring Fe atoms, which influences the interaction of Fe atoms [12]. The small interaction strength of Fe atoms will diminish the energy difference of the down-spin and up-spin electrons and make the Fermi level of the down-spin band touches the top of the up-spin band. The $N_\uparrow$ is not constant and the alloy become magnetically weak. Therefore, the actual $\overline{\mu}$ of Fe-based MGs is different from that calculated with our simple model could be due to the local structural effect as pointed out by Friedel.

For most of the studied Fe-based MGs, the calculated $\overline{\mu}$stays above the grey dashed trend line and the deviation widens as the Fe concentration decreases, as shown in Fig. 3 (the dashed red line). The phenomenon that the calculated $\overline{\mu}$ is larger than the actual value is herein attributed to the magnetic weakness of the closed packed Fe atoms in an amorphous structure, particularly with the reduction of the Fe concentration [18]. The calculated $\overline{\mu}$'s of $(Fe_{0.76}Si_{0.096}B_{0.084}P_{0.06})_{96}Mo_4$ and $(Fe_{0.76}Si_{0.096}B_{0.084}P_{0.06})_{94}Mo_6$ MGs lie far above the red dashed trend line (the circled data with

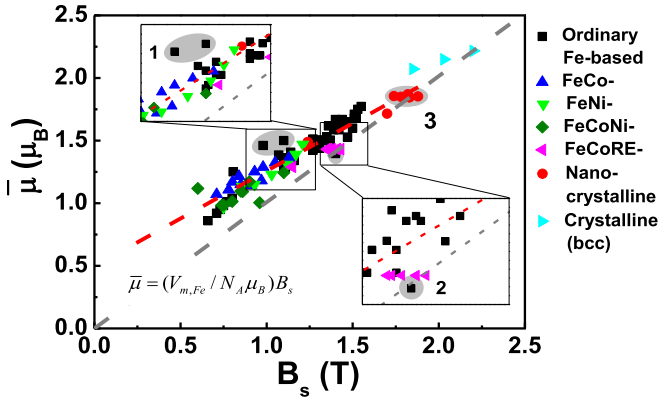

Fig. 3. The calculated $\bar{\mu}$ versus B_s for the studied MGs. The grey dashed line represents $\bar{\mu}=(V_{m,Fe}/N_A\mu_B)B_s$. The red dashed line is the guide for the eyes. (A single column fitting image.). (For interpretation of the references to colour in this figure legend, the reader is referred to the web version of this article.)

the label "1" in Fig. 3), which could be caused by the formation of densely packed Fe local structures inducing the reduction of the interaction of Fe atoms [26]. On the other hand, the $\bar{\mu}$ of $(Fe_{0.75}B_{0.15}Si_{0.10})_{96}Nb_4$ MG lies far below the red dashed trend line (the circled data with the label "2" in Fig. 3), signaling an opposite effect in the presence of a high concentration of small atoms (B, Si). This could be associated with the small molar volume of the small atoms. For the FeCoRE-based MGs, the calculated $\bar{\mu}$ is also close to the experimental measurement. This may be due to the large atomic radius of rare-earth (RE) element, the alloying of which leads to the widening of the distance of neighboring Fe atoms and thus a local packing configuration close to bcc α-Fe with strong ferromagnetism [12].

FeCu-based nanocrystalline alloys are composed of almost pure bcc Fe, almost Cu-free amorphous phase and Cu-rich clusters [11]. For the Cu-free Fe-based amorphous phase the spin-up energy band gap of Fe cannot be smeared by the small concentration of impurities. Both the Cu-free amorphous phase and bcc-Fe nanocrystallites are magnetically strong. We regard that free electrons can still transfer between bcc Fe, amorphous phase and Cu-rich clusters in the FeCu-based alloys. Thus, the calculated $\bar{\mu}$ is consistent very well with the free electron rule for Cu alloyed Fe-based nanocrystalline alloys with a high concentration of Fe, as shown in Fig. 3 (the circled data with the label "3"). The free electron rule is applicable for $Fe_{90}Zr_7B_3$ nanocrystalline alloy and Fe-based crystalline alloys due to their strong magnetism.

2.3. Glass forming ability, saturated magnetization and local short-range order

Based on the above discussions, it is clear that the difference between the calculated $\bar{\mu}$ and the experimental measurement is related to the local packing environment of ferromagnetic atoms besides the smearing effect of the energy gap by impurities for MGs. Since the glass forming ability (GFA) of MGs is also affected by the local packing of solvent or solute atoms [20–22], we are now at a position to assess the possible correlation between GFA and saturated magnetism of the soft-magnetic MGs. Parameters like ΔT_x ($\Delta T_x = T_x - T_g$, where T_x is the onset crystallization temperature of the glass) [27], γ [$\gamma = T_x/(T_g + T_l)$] [28] and α ($\alpha = T_x/T_l$) [29] can be used for describing the glass forming ability of liquids. For simplicity, we here quantify the GFA of various MGs with the reduced glass transition temperature T_{rg} proposed early by Turnbull which is suitable and often used for Fe-based MGs [30]. Table 2 lists the T_{rg} and $B_{s,cal}$- B_s of the variety of soft magnetic MGs, where $B_{s,cal}$ stands for the calculated saturated magnetization using Eq. (1) (For the convenience of discussions, the studied Fe-based MGs are divided into Mo1, Mo2, Mo3, Nb1, Nb2, Ga, Tb, Co and Ni systems according to the alloyed element). Fig. 4 shows the plot of T_{rg} versus $B_{s,cal}$- B_s for the variety of Fe-based soft-magnetic MGs, from which it can be found that T_{rg} decreases with the increase of $B_{s,cal}$- B_s for the Fe-based MG alloyed with Mo, Nb and Ga (Fig. 4(a)). This phenomenon indicates that, in these particular Fe-based MGs, the higher is the GFA the better does the ideal Friedel's picture fit the experimental results and thus the stronger is the ferromagnetism. In contrast, T_{rg} increases with the increase of $B_{s,cal}$- B_s when the Fe-based MG is alloyed with Tb or Co (Fig. 4(b)); furthermore, there seems no correlation between $B_{s,cal}$- B_s and T_{rg} when the Fe-based MG is alloyed with Ni (Fig. 4(c)). These behaviors could be rationalized from the perspective of exchange interacting strength of

Table 2
The calculated saturated magnetization $B_{s,cal}$, $B_{s,cal} - B_s$ and T_{rg} for a series of Fe-based MGs.

Composition	$B_{s,cal}$ (T)	$B_{s,cal}$-B_s (T)	T_{rg}
Mo1 [34]			
$Fe_{79}P_{10}C_4B_4Si_3$	1.75	0.22	0.586
$Fe_{78}Mo_1P_{10}C_4B_4Si_3$	1.67	0.23	0.585
$Fe_{77}Mo_2P_{10}C_4B_4Si_3$	1.58	0.19	0.587
$Fe_{76}Mo_3P_{10}C_4B_4Si_3$	1.50	0.18	0.6
$Fe_{75}Mo_4P_{10}C_4B_4Si_3$	1.42	0.15	0.613
$Fe_{74}Mo_5P_{10}C_4B_4Si_3$	1.34	0.20	0.6
Mo2 [35]			
$Fe_{76}C_{7.0}Si_{3.3}B_5P_{8.7}Mo_0$	1.68	0.16	0.603
$Fe_{75}C_{7.0}Si_{3.3}B_5P_{8.7}Mo_1$	1.60	0.19	0.604
$Fe_{73}C_{7.0}Si_{3.3}B_5P_{8.7}Mo_3$	1.44	0.14	0.618
$Fe_{71}C_{7.0}Si_{3.3}B_5P_{8.7}Mo_5$	1.27	0.17	0.615
Mo3 [26]			
$(Fe_{0.76}Si_{0.096}B_{0.084}P_{0.06})_{100}Mo_0$	1.68	0.17	0.571
$(Fe_{0.76}Si_{0.096}B_{0.084}P_{0.06})_{98}Mo_2$	1.53	0.18	0.572
$(Fe_{0.76}Si_{0.096}B_{0.084}P_{0.06})_{96}Mo_4$	1.49	0.39	0.56
$(Fe_{0.76}Si_{0.096}B_{0.084}P_{0.06})_{94}Mo_6$	1.46	0.48	0.538
Nb1 [41]			
$(Fe_{75}B_{15}Si_{10})_{99}Nb_1$	1.59	0.09	0.56
$(Fe_{75}B_{15}Si_{10})_{98}Nb_2$	1.53	0.06	0.57
$(Fe_{75}B_{15}Si_{10})_{96}Nb_4$	1.39	−0.01	0.61
Nb2 [36]			
$(Fe_{0.39}Ni_{0.39}B_{0.16}P_{0.06})_{99}Nb_1$	1.04	0.24	0.535
$(Fe_{0.39}Ni_{0.39}B_{0.16}P_{0.06})_{98.5}Nb_{1.5}$	1.01	0.24	0.543
$(Fe_{0.39}Ni_{0.39}B_{0.16}P_{0.06})_{98}Nb_2$	0.98	0.23	0.555
$(Fe_{0.39}Ni_{0.39}B_{0.16}P_{0.06})_{97.5}Nb_{2.5}$	0.95	0.22	0.581
$(Fe_{0.39}Ni_{0.39}B_{0.16}P_{0.06})_{97}Nb_3$	0.92	0.21	0.571
$(Fe_{0.39}Ni_{0.39}B_{0.16}P_{0.06})_{96}Nb_4$	0.86	0.20	0.57
Ga [45]			
$Fe_{77}Ga_3P_{9.5}C_4B_4Si_{2.5}$	1.61	0.25	0.6
$Fe_{78}Ga_2P_{9.5}C_4B_4Si_{2.5}$	1.67	0.27	0.59
Tb [38]			
$(Fe_{0.74}Tb_{0.01}B_{0.2}Si_{0.05})_{96}Nb_4$	1.34	0.20	0.573
$(Fe_{0.73}Tb_{0.02}B_{0.2}Si_{0.05})_{96}Nb_4$	1.29	0.28	0.586
$(Fe_{0.72}Tb_{0.03}B_{0.2}Si_{0.05})_{96}Nb_4$	1.24	0.32	0.605
$(Fe_{0.71}Tb_{0.04}B_{0.2}Si_{0.05})_{96}Nb_4$	1.19	0.43	0.622
$(Fe_{0.70}Tb_{0.05}B_{0.2}Si_{0.05})_{96}Nb_4$	1.14	0.45	0.67
$(Fe_{0.69}Tb_{0.06}B_{0.2}Si_{0.05})_{96}Nb_4$	1.09	0.48	0.675
$(Fe_{0.68}Tb_{0.07}B_{0.2}Si_{0.05})_{96}Nb_4$	1.04	0.52	0.667
Co [49]			
$[(Fe_{0.9}Co_{0.1})_{0.75}B_{0.2}Si_{0.05}]_{96}Nb_4$	1.36	0.23	0.57
$[(Fe_{0.8}Co_{0.2})_{0.75}B_{0.2}Si_{0.05}]_{96}Nb_4$	1.32	0.27	0.58
$[(Fe_{0.7}Co_{0.3})_{0.75}B_{0.2}Si_{0.05}]_{96}Nb_4$	1.28	0.30	0.586
$[(Fe_{0.6}Co_{0.4})_{0.75}B_{0.2}Si_{0.05}]_{96}Nb_4$	1.25	0.32	0.586
$[(Fe_{0.5}Co_{0.5})_{0.75}B_{0.2}Si_{0.05}]_{96}Nb_4$	1.21	0.37	0.587
Ni [39]			
$Fe_{76}Mo_{3.5}P_{10}C_4B_4Si_{2.5}$	1.47	0.26	0.56
$Fe_{71}Ni_5Mo_{3.5}P_{10}C_4B_4Si_{2.5}$	1.39	0.22	0.561
$Fe_{66}Ni_{10}Mo_{3.5}P_{10}C_4B_4Si_{2.5}$	1.31	0.19	0.536
$Fe_{61}Ni_{15}Mo_{3.5}P_{10}C_4B_4Si_{2.5}$	1.23	0.20	0.522
$Fe_{56}Ni_{20}Mo_{3.5}P_{10}C_4B_4Si_{2.5}$	1.15	0.22	0.507

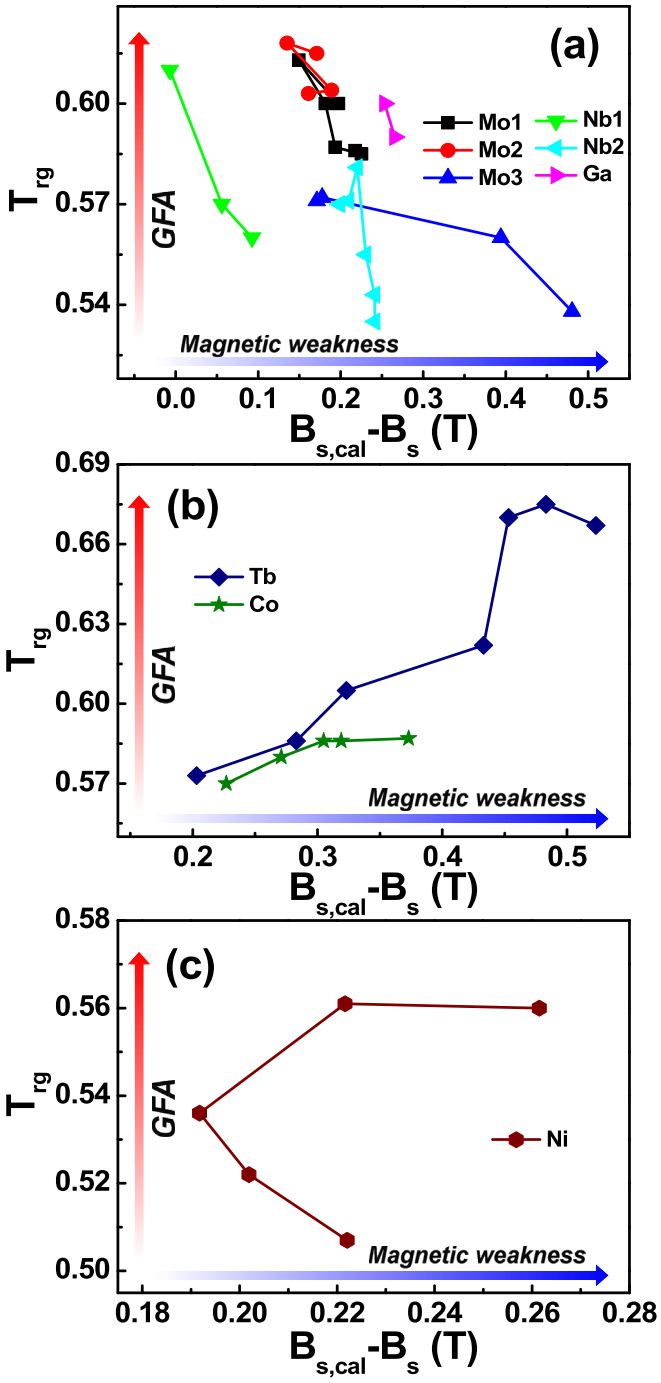

Fig. 4. The T_{rg} versus $B_{s,cal} - B_s$ for (a) Mo1, Mo2, Mo3, Nb1, Nb2, Ga Fe-based MGs; (b) Tb, Co Fe-based MGs; (c) Ni Fe-based MGs. (A single column fitting image.)

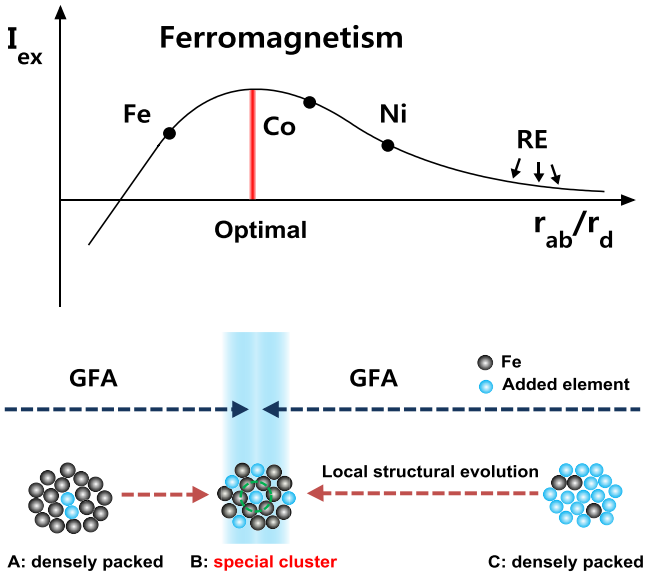

Fig. 5. Top: the r_{ab}/r_d dependent exchange strength I_{ex} for Fe, Co, Ni and rare earth elements. Bottom: The evolution of the local structure with the change of the composition. (A two-column fitting image.)

ferromagnetic atoms, which suggests the crucial role of atomic packing for both saturated magnetization and GFA, as discussed in the following text.

As shown in the top panel of Fig. 5, the exchange interacting strength I_{ex} of Fe atoms in an alloy is determined by the ratio r_{ab}/r_d, where r_{ab} and r_d stand for the interatomic distance between neighboring Fe atoms and the radius of d-orbit of Fe, respectively [31]. In crystalline α-Fe, the ratio r_{ab}/r_d is known to be smaller than the optimal value for the largest I_{ex}. This ratio becomes even smaller in the densely packed amorphous Fe, thereby resulting in the small I_{ex} or magnetic weakness according to the Stoner model [32]. When nonmagnetic elements are alloyed into the amorphous Fe, r_{ab} can change due to the local structural packing around the Fe atoms, as shown in the bottom panel of Fig. 5. If the alloying brings about solute-centered short-range order, as illustrated in Fig. 5, and thus locally increases the ratio r_{ab}/r_d, which becomes closer to the optimal value for the maximized I_{ex}, the ferromagnetism should be strengthened in the MG, as reflected by the decrease of $B_{s,cal}$- B_s. Furthermore, if such short-range order behaves as a "glass stabilizer", just like the icosahedra short-range order to Zr-based MGs [33], GFA can be also improved via the formation of such short-range order. As a result, GFA increases with ferromagnetic strength as the solvent Fe atoms become more separated around the solute-centered clusters (marked as the green dashed circle in Fig. 5) [20–22]. Following this line of reasoning, the simultaneous increase of GFA and ferromagnetism in the Fe-based MGs alloyed with Mo, Nb and Ga as shown in Fig. 4(a) suggests that the solute-centered clusters must act as both "glass stabilizers" and "solvent separators".

Different from the cases of alloying Mo, Nb and Ga, T_{rg} increases with $B_{s,cal}$- B_s if the Fe-based MG is alloyed of Tb and Co. This indicates that the GFA of these alloys reduces as their ferromagnetic strength increases. As shown in the up panel of Fig. 5, the ratio r_{ab}/r_d of Tb, Co and Ni is larger than the optimum value for the largest I_{ex} in a densely packed structure [31]. When the alloying element Tb or Co forms glass-stabilizing solute-centered clusters, which imparts the MG with the best GFA, the neighboring distance of Tb and Co atoms is enlarged. Consequently, the I_{ex} of the alloying elements is reduced, which leads to the increase of $B_{s,cal}$- B_s, i. e., the increase of magnetic weakness. Following this line of reasoning, the lack of correlation between $B_{s,cal}$- B_s and T_{rg} for the Fe-based MG alloyed with less than 20% Ni is probably due to a competition between the two mechanisms aforementioned, i. e., the changes of the neighboring Ni atomic distance and the neighboring Fe distance.

To further justify the above opinions, it is worth noting that the competing primary crystalline phases of the Mo1, Mo2 systems are both fcc $(Fe,Mo)_{23}(B,C)_6$ phase with a lattice parameter larger than 1 nm including 116 atoms in the unit cell [34,35]. The primary crystalline phase in the Nb2 system is $(Fe,Ni,Nb)_{23}B_6$ which also has

a fcc $Fe_{23}B_6$ type structure with the replacement of Fe by Ni and Nb [36,37]. The precipitation phases for the Tb system annealed at 1023 K are $Fe_{23}B_6$ and $Tb_2Fe_{14}B$ phases [38]. The XRD pattern of the Ni system annealed at 768 K for 1800 s indicates the coexistence of α-Mn type phases and $(Fe,Ni,Mo)_{23}(B,C)_6$ phase [39]. These results support that the GFA of these MGs are associated with the existence of the densely packed clusters containing the solute element and the solvent element.

3. Conclusions

To conclude, we propose a set of simple rules in this work for the calculation of $\overline{\mu}$ of different soft magnetic Fe-based alloys based on the idea that free electrons can transfer between the metallic elements with different E_F, thus change the $\overline{\mu}$ and B_s of the Fe-based alloys. Given $B_s = N_A\overline{\mu}\mu_B/V_m$, small atoms are beneficial for B_s as they can significantly reduce the alloy's molar volume V_m. This may explain the common practice that small atoms, like Si, B, and high-E_F atoms, like Co, Ni, Cu, are usually alloyed into the Fe-based alloys to enhance B_s. Furthermore, we found that the departure of B_s calculated from our simple rules can be attributed to the intrinsic magnetic weakness associated with local atomic packing in the amorphous structure. Based on the data reported in the literature, it can be inferred that large-sized alloying atoms which could separate neighboring Fe atoms to a greater distance can reduce the ferromagnetic weakness of the Fe-based MG. Interestingly, such a departure can be correlated, either positively or negatively, with the GFA of the Fe-based soft magnetic MG, therefore implicative of an inherent connection of B_s and GFA originating from the local short-range structure in the Fe-based MGs.

Acknowledgements

The financial supports of the General Research Fund (GRF) of Hong Kong (No. CityU9042066 and No. CityU9041863) are acknowledged.

References

[1] C. Suryanarayana, A. Inoue, Iron-based bulk metallic glasses, Inter. Mater. Rev. 58 (2013) 131–166.
[2] P. Tiberto, M. Baricco, E. Olivetti, R. Piccin, Magnetic properties of bulk metallic glasses, Adv. Eng. Mater. 9 (2007) 468–474.
[3] F.E. Luborsky, Magnetic properties of amorphous alloys, J. Magn. Magn. Mater. 7 (1978) 143–149.
[4] R.C. O'Handley, Physics of ferromagnetic amorphous alloys, J. Appl. Phys. 62 (1987) R15.
[5] C.D. Graham Jr., T. Egami, Magnetic properties of amorphous alloys, Ann. Rev. Mater. Sci. 8 (1978) 423–457.
[6] H. Kronmüller, M. Fähnle, M. Domann, H. Grimm, R. Grimm, B. Gröger, Magnetic properties of amorphous ferromagnetic alloys, J. Magn. Magn. Mater. 13 (1979) 53–70.
[7] Y. Yoshizawa, S. Oguma, K. Yamauchi, New Fe-based soft magnetic alloys composed of ultrafine grain structure, J. Appl. Phys. 64 (1988) 6044–6046.
[8] R. Hasegawa, Advances in amorphous and nanocrystalline magnetic materials, J. Magn. Magn. Mater. 304 (2006) 187–191.
[9] Y.R. Zhang, R.V. Ramanujan, The effect of Copper alloying additions on the crystallization of an amorphous Fe–Si–B alloy, J. Mater. Sci. 41 (2006) 5292–5301.
[10] M. Ohta, Y. Yoshizawa, Cu addition effect on soft magnetic properties in Fe–Si–B alloy system, J. Appl. Phys. 103 (2008) 07E722.
[11] A. Makino, H. Men, T. Kubota, K. Yubuta, A. Inoue, FeSiBPCu nanocrystalline soft magnetic alloys with high Bs of 1.9 Tesla produced by crystallizing hetero-amorphous phase, Mater. Trans. 50 (2009) 204–209.
[12] Y. Kakehashi, Modern Theory of Magnetism in Metals and Alloys, Springer, Berlin, 2013.
[13] R. Alben, J.I. Budnick, G.S. Cargill III, In Metallic Glasses, American Society for Metals, Metals Park, Ohio, 1978.
[14] J. Friedel, Metallic alloys, Nuovo Cimento (Suppl. 7) (1958) 287–311.
[15] A.P. Malozemoff, A.R. Williams, V.L. Moruzzi, "Band-gap theory" of strong ferromagnetism: application to concentrated crystalline and amorphous Fe- and Co-metalloid alloys, Phys. Rev. B 29 (1984) 1620–1632.
[16] K. Yamauchi, T. Mizoguchi, The magnetic moments of amorphous metal-metalloid alloys, J. Phys. Soc. Jpn. 39 (1975) 541.
[17] A.R. Williams, V.L. Moruzzi, A.P. Malozemoff, K. Terakura, Generalized Slater-Pauling curve for transition-metal magnets, IEEE Trans. Magn. 19 (1983) 1983.
[18] A.P. Malozemoff, A.R. Williams, K. Terakura, V.L. Moruzzi, K. Fukamichi, Magnetism of amorphous metal-metal alloys, J. Magn. Magn. Mater. 35 (1983) 192–198.
[19] Y. Kakehashi, S. Akbar, N. Kimura, Molecular-dynamics approach to itinerant magnetism with complex magnetic structures, Phys. Rev. B 57 (1998) 8354.
[20] X.K. Xi, L.L. Li, B. Zhang, W.H. Wang, Y. Wu, Correlation of atomic cluster symmetry and glass-forming ability of metallic glass, Phys. Rev. Lett. 99 (2007) 095501.
[21] H.L. Peng, M.Z. Li, W.H. Wang, C.Z. Wang, K.M. Ho, Effect of local structures and atomic packing on glass forming ability in Cu_xZr_{100-x} metallic glasses, Appl. Phys. Lett. 96 (2010) 021901.
[22] L. Yang, G.-Q. Guo, Structural origin of the high glass-forming ability in Gd doped bulk metallic glasses, Appl. Phys. Lett. 97 (2010) 091901.
[23] Y. Li, Q. Guo, J.A. Kalb, C.V. Thompson, Matching glass-forming ability with the density of the amorphous phase, Science 322 (2008) 1816–1819.
[24] H.B. Yu, W.H. Wang, H.Y. Bai, An electronic structure perspective on glass-forming ability in metallic glasses, Appl. Phys. Lett. 96 (2010) 081902.
[25] H.B. Michaelson, The work function of the elements and its periodicity, J. Appl. Phys. 48 (1977) 4729.
[26] X. Li, C. Qin, H. Kato, A. Makino, A. Inoue, Mo microalloying effect on the glass-forming ability, magnetic, mechanical and corrosion properties of $(Fe_{0.76}Si_{0.096}B_{0.084}P_{0.06})$100-xMox bulk glassy alloys, J. Alloys Compd. 509 (2011) 7688–7691.
[27] A. Inoue, T. Zhang, T. Masumoto, Glass-forming ability of alloys, J. Non cryst. Solids 156 (1993) 473–480.
[28] Z.P. Lu, C.T. Liu, Glass formation criterion for various glass-forming systems, Phys. Rev. Lett. 91 (2003) 115505.
[29] K. Mondal, B.S. Murty, On the parameters to assess the glass forming ability of liquids, J. Non cryst. Solids 351 (2005) 1366–1371.
[30] D. Turnbull, Under what conditions can a glass be formed? Contem. Phys. 10 (1969) 473–488.
[31] R.E. Hummel, Electronic Properties of Materials, fourth ed., Springer, New York, 2011.
[32] J. Stöhr, H.C. Siegmann, Magnetism. From Fundamentals to Nanoscale Dynamics, Springer, Berlin, 2006.
[33] S.F. Chen, C.Y. Hung, S.J. Wang, S.H. Chen, C.C. Chen, Influence of annealing treatment on soft magnetic properties of Fe76Si10B10Cr2Y2 amorphous ribbon, J. Alloys Compd. 627 (2015) 333–336.
[34] B. Shen, M. Akiba, A. Inoue, Excellent soft-ferromagnetic bulk glassy alloys with high saturation magnetization, Appl. Phys. Lett. 88 (2006) 131907.
[35] Z.B. Jiao, H.X. Li, Y. Wu, J.E. Gao, S.L. Wang, S. Yi, Z.P. Lu, Effects of Mo additions on the glass-forming ability and magnetic properties of bulk amorphous Fe-C-Si-B-P-Mo alloys, Sci. China Phys. Mech. Astron. 53 (2010) 430–434.
[36] A. Wang, M. Zhang, J. Zhang, H. Men, B. Shen, S. Pang, T. Zhang, FeNiPBNb bulk glassy alloys with good soft-magnetic properties, J. Alloys Compd. 536 (2012) S354–S358.
[37] M. Imafuku, S. Sato, H. Koshiba, E. Matsubara, A. Inoue, Structural variation of Fe-Nb-B metallic glasses during crystallization process, Scr. Mater. 44 (2001) 2369–2372.
[38] J.W. Li, A.N. He, B.L. Shen, Effect of Tb addition on the thermal stability, glass-forming ability and magnetic properties of Fe–B–Si–Nb bulk metallic glass, J. Alloys Compd. 586 (2014) S46–S49.
[39] M. Zhang, A. Wang, B. Shen, Enhancement of glass-forming ability of Fe-based bulk metallic glasses with high saturation magnetic flux density, AIP Adv. 2 (2012) 022169.
[40] B. Shen, M. Akiba, A. Inoue, Effects of Si and Mo additions on glass-forming inFeGaPCBbulk glassy alloys with high saturation magnetization, Phys. Rev. B 73 (2006).
[41] A. Inoue, B. Shen, New Fe-based bulk glassy alloys with high saturated magnetic flux density of 1.4–1.5T, Mater. Sci. Eng. A 375–377 (2004) 302–306.
[42] A. Inoue, Y. Shinohara, J.S. Gook, Thermal and magnetic properties of bulk Fe-based glassy alloys prepared by copper mold casting, Mater. Trans. JIM 36 (1995) 1427–1433.
[43] C.Y. Lin, T.S. Chin, S.X. Zhou, Z.C. Lu, L. Wang, F.F. Chen, M.X. Pan, W.H. Wang, Magnetic properties and glass-forming ability of modified Fe–P–Si–B bulk amorphous alloys, J. Magn. Magn. Mater. 282 (2004) 156–162.
[44] B. Shen, H. Kimura, A. Inoue, T. Mizushima, Bulk glassy Fe-Ga-PCB alloys with high saturation magnetization and good soft magnetic properties synthesized by fluxing treatment and copper mold casting, Mater. Trans. 42 (2001) 660–663.
[45] B. Shen, A. Inoue, Bulk glassy Fe-Ga-PCB-Si alloys with high glass-forming ability, high saturation magnetization and good soft magnetic properties, Mater. Trans. 43 (2002) 1235–1239.
[46] M. Shi, Z. Liu, T. Zhang, Effects of minor Sn addition on the glass formation and properties of Fe-metalloid metallic glasses with high magnetization and high glass forming ability, J. Magn. Magn. Mater. 378 (2015) 417–423.
[47] D.S. Song, J.H. Kim, E. Fleury, W.T. Kim, D.H. Kim, Synthesis of ferromagnetic Fe-based bulk glassy alloys in the Fe–Nb–B–Y system, J. Alloys Compd. 389 (2005) 159–164.
[48] H.X. Li, H.Y. Jung, S. Yi, Glass forming ability and magnetic properties of bulk metallic glasses Fe68.7–xC7.0Si3.3B5.5P8.7Cr2.3Mo2.5Al2.0Cox (x=0–10), J. Magn. Magn. Mater. 320 (2008) 241–245.

[49] B. Shen, A. Inoue, C. Chang, Superhigh strength and good soft-magnetic properties of (Fe,Co)–B–Si–Nb bulk glassy alloys with high glass-forming ability, Appl. Phys. Lett. 85 (2004) 4911.
[50] B. Shen, C. Chang, T. Kubota, A. Inoue, Superhigh strength and excellent soft-magnetic properties of $[(Co_{1-x}Fe_x)_{0.75}B_{0.2}Si_{0.05}]_{96}Nb_4$ bulk glassy alloys, J. Appl. Phys. 100 (2006) 013515.
[51] W. Zhang, A. Inoue, Soft magnetic properties of (Fe, Co)-RE-B amorphous alloys with a large supercooled liquid region, Mater. Trans. 42 (2001) 1142–1145.
[52] W. Zhang, Y. Long, M. Imafuku, A. Inoue, Thermal stability and soft magnetic properties of (Fe, Co)-(Nd, Dy)-B glassy alloys with high boron concentrations, Mater. Trans. 43 (2002) 1974–1978.
[53] Q. Li, Formation of ferromagnetic bulk amorphous Fe 40 Ni 40 P 14 B 6 alloys, Mater. Lett. 60 (2006) 3113–3117.
[54] Z. Gan, H. Yi, J. Pu, J. Wang, J. Xiao, Preparation of bulk amorphous Fe–Ni–P–B–Ga alloys from industrial raw materials, Scr. Mater. 48 (2003) 1543–1547.
[55] A. Inoue, T. Zhang, A. Takeuchi, Bulk amorphous alloys with high mechanical strength and good soft magnetic properties in Fe–TM–B (TM= IV–VIII group transition metal) system, Appl. Phys. Lett. 71 (1997) 464–466.
[56] B. Shen, C. Chang, Z. Zhang, A. Inoue, Enhancement of glass-forming ability of FeCoNiBSiNb bulk glassy alloys with superhigh strength and good soft-magnetic properties, J. Appl. Phys. 102 (2007) 023515.
[57] B. Shen, C. Chang, A. Inoue, Formation, ductile deformation behavior and soft-magnetic properties of (Fe,Co,Ni)–B–Si–Nb bulk glassy alloys, Intermetallics 15 (2007) 9–16.
[58] X.D. Fan, H. Men, A.B. Ma, B.L. Shen, Soft magnetic properties in Fe84–xB10C6Cux nanocrystalline alloys, J. Magn. Magn. Mater. 326 (2013) 22–27.
[59] F. Kong, A. Wang, X. Fan, H. Men, B. Shen, G. Xie, A. Makino, A. Inoue, High Bs Fe84–xSi4B8P4Cux ($x = 0 - 1.5$) nanocrystalline alloys with excellent magnetic softness, J. Appl. Phys. 109 (2011) 07A303.
[60] F. Kong, H. Men, T. Liu, B. Shen, Effect of P to B concentration ratio on soft magnetic properties in FeSiBPCu nanocrystalline alloys, J. Appl. Phys. 111 (2012) 07A311.